Investigation of the radially resolved oxygen dissociation degree and local mean electron energy in oxygen plasmas in contact with different surface materials

T. Tsutsumi, A. Greb, A. R. Gibson, M. Hori, D. O'Connell, and T. Gans

Citation: Journal of Applied Physics **121**, 143301 (2017); doi: 10.1063/1.4979855
View online: http://dx.doi.org/10.1063/1.4979855
View Table of Contents: http://aip.scitation.org/toc/jap/121/14
Published by the American Institute of Physics

Investigation of the radially resolved oxygen dissociation degree and local mean electron energy in oxygen plasmas in contact with different surface materials

T. Tsutsumi,[1] A. Greb,[2] A. R. Gibson,[2] M. Hori,[1] D. O'Connell,[2] and T. Gans[2]
[1]*Graduate School of Engineering, Nagoya University, Nagoya 464-8603, Japan*
[2]*York Plasma Institute, Department of Physics, University of York, Heslington, York YO10 5DD, United Kingdom*

(Received 13 June 2016; accepted 24 March 2017; published online 10 April 2017)

Energy Resolved Actinometry is applied to simultaneously measure the radially resolved oxygen dissociation degree and local mean electron energy in a low-pressure capacitively coupled radio-frequency oxygen plasma with an argon tracer gas admixture. For this purpose, the excitation dynamics of three excited states, namely, Ar($2p_1$), O($3p^3P$), and O($3p^5P$), were determined from their optical emission at 750.46 nm, 777.4 nm, and 844.6 nm using Phase Resolved Optical Emission Spectroscopy (PROES). Both copper and silicon dioxide surfaces are studied with respect to their influence on the oxygen dissociation degree, local mean electron energy, and the radial distributions of both quantities and the variation of the two quantities with discharge pressure and driving voltage are detailed. The differences in the measured dissociation degree between different materials are related back to atomic oxygen surface recombination probabilities. [http://dx.doi.org/10.1063/1.4979855]

I. INTRODUCTION

Oxygen plasmas have been widely applied in industry for a variety of different surface modifications such as photoresist removal, chemical vapour deposition, and oxidation.[1–5] To realize a process where these modifications are reproducible and uniform over a large area, plasma control techniques capable of tailoring the properties of the plasma, including the mean electron energy and reactive species densities, are crucial.[6–11] Of particular importance in this context are the radial distributions of both quantities. Furthermore, the wafer material itself and the condition of the other wall materials in the reactor affect the absolute number densities of reactive species due to wall loss processes, the probability for which is dependent on many factors.[12–25] This makes it particularly difficult to accurately control the densities of highly reactive species, such as atomic oxygen, in industrial processing applications. Previous investigations have sought insight into these processes by measuring the density of atomic oxygen and its surface recombination probability for various materials using two-photon absorption laser-induced fluorescence (TALIF),[12,26–30] optical emission spectroscopy (OES),[21,22,31–34] and VUV absorption spectroscopy.[23,35,36] TALIF and VUV absorption are well known for their accuracy, however, both are challenging to implement in industrial plasma reactors, particularly if spatially resolved measurements are required. Optical emission spectroscopy on the other hand has the advantage of being completely non-invasive and easily allows for spatially resolved measurements which are key for understanding radial variations in plasma parameters which are important for uniformity in processing applications. The conventional approach to measuring reactive species densities using OES, known as actinometry, is based on observing the time averaged emission from a plasma incorporating an inert trace gas admixture, such as argon. Where the population of a given excited state is dominated by electron impact excitation the time averaged emission intensity from the excited state of interest at a given wavelength is defined as

$$\langle I \rangle_{rf} = \frac{1}{4\pi} h\upsilon a_{ik} \langle k_e n_e \rangle_{rf} n_0. \tag{1}$$

Here, $h\upsilon$ denotes the photon energy, k_e is the excitation rate coefficient, n_e is the electron density, and n_0 is the species ground state density. The factor $1/4\pi$ accounts for the solid angle of emission of isotropic radiation. a_{ik} is the optical branching ratio defined as

$$a_{ik} = \frac{A_{ik}}{A_i + Q_i}. \tag{2}$$

Here, A_i is the sum over all optical transition probabilities A_{ik} from the excited state i to lower states k and Q_i is the non-radiative collisional quenching rate of the excited state given by

$$Q_i = \sum_q k_{iq} n_q. \tag{3}$$

Here, k_{iq} denotes the rate coefficient for collisional quenching of the excited state i through collisions with species of density n_q. In the first approximation, the density of a reactive species can be estimated through measuring the emission intensity of an excited state of the reactive species and dividing by the emission intensity of an excited state of the tracer gas, which has a known density, and rearranging for the ground state density of the reactive species of interest (this is represented by the first term on the right hand side of Eq. (4)). This process can be carried out easily by choosing

suitable emission lines of both the reactive species and the tracer gas such that the electron impact threshold energy and energy dependence of the excitation rates k_e are similar in both cases. If these criteria are satisfied, the electron energy dependences cancel upon division leaving a constant due to the difference in the absolute value of each rate. However, while easy to implement the described procedure can be susceptible to significant error as the assumptions of similar electron impact energy thresholds and energy dependences of the excitation rates are rarely fulfilled.

In the case of atomic oxygen, the described concept is complicated further by the fact that excited states of atomic oxygen can also arise due to dissociative excitation of ground state molecular oxygen through electron impact.[37] In this case, the simple assumptions that the threshold energy and the energy dependence of the excitation rates of both excited states are similar does not apply as the electron impact cross section for dissociative excitation is significantly different in shape and magnitude from that due to direct excitation. Various works have extended the basic actinometry approach for atomic oxygen (and atomic hydrogen[38]) to incorporate the dissociative excitation process.[32–34] In order to do this, argon is typically used as a tracer gas with the emission from the $Ar(2p_1)$ state monitored at $\lambda = 750.46$ nm. The corresponding atomic oxygen emission from the $O(3p^3P)$ state is monitored at $\lambda = 844.6$ nm. In order to determine the atomic oxygen density, the expression for the emission intensity from the $O(3p^3P)$ state at $\lambda = 844.6$ nm can then be extended to incorporate dissociative excitation. The resulting expression for the atomic oxygen density is given as

$$n_O = \frac{I_O}{I_{Ar}} \frac{h\upsilon_{Ar}}{h\upsilon_O} \frac{k^*_{Ar,d}}{k^*_{O,d}} \frac{a_{ik,Ar}}{a_{ik,O}} n_{Ar} - \frac{k^*_{O,de}}{k^*_{O,d}} n_{O2}, \tag{4}$$

where

$$k^* = \frac{\langle k_e n_e \rangle_{rf}}{\langle n_e \rangle_{rf}}. \tag{5}$$

The first term on the right hand side of Eq. (4) corresponds to the basic actinometry approach, while the second term represents the extension accounting for dissociative excitation. The direct and dissociative excitation rate coefficients are denoted by the subscripts d and de, respectively. In the above form, accurate results can only be obtained when the dominant sources of production of the considered excited states are via electron impact with ground state atomic and molecular oxygen. However, recent publications have detected the presence of significant quantities of vibrationally[39] and electronically excited states[40] of molecular oxygen in oxygen plasmas. If the electron impact cross sections for dissociative excitation from these states into the $O(3p^3P)$ state were to be significant, this may affect the atomic oxygen densities derived via actinometry. Quantitative consideration of these effects is difficult given the lack of data for electron impact dissociative excitation of vibrationally or electronically excited states and as a result, these effects are not considered here.

As mentioned before, when dissociative excitation is accounted for the thresholds and energy dependences of the corresponding rate coefficients cannot be assumed to cancel upon division. Instead, the rate coefficients must be calculated directly from their electron impact cross sections through the mean electron energy and the corresponding electron energy distribution function (EEDF) of the plasma which has to be either assumed or calculated numerically. Several works have demonstrated this coupling of experimental observations and simulations to be a reliable method of determining the atomic oxygen density in both high and low pressure plasma sources.[32–34]

Here, we apply a further extension of the described techniques, known as Energy Resolved Actinometry (ERA) in order to measure atomic oxygen densities and local mean electron energies simultaneously and with high spatial resolution. This technique has been described in detail and benchmarked for the case of an atmospheric pressure plasma jet by Greb *et al.*[41] Briefly, the ERA approach, which is inclusive of direct and dissociative excitation processes, modifies the commonly used actinometry technique in two significant ways (i) to additionally include atomic oxygen emission from the $O(3p^5P)$ excited state at $\lambda = 777.4$ nm and (ii) to utilise excitation ratios in place of emission intensity ratios. The required excitation ratios are measured experimentally using Phase Resolved Optical Emission Spectroscopy (PROES) which allows for nanosecond temporal resolution of the plasma emission and therefore the derivation of the excitation rates for individual excited states. This is discussed further in Section III. The derived excitation ratios are then compared with those calculated through EEDFs obtained using the two-term Boltzmann equation solver BOLSIG+.[42] By varying the dissociation degree and the mean electron energy in the Boltzmann solver calculations, the simulated excitation ratios can be varied in order to match those observed experimentally, allowing the experimental dissociation degree and mean electron energy to be inferred. The absolute atomic oxygen density is then easily calculated via the ideal gas law through either measurement or assumption of the gas temperature.

In order to account for direct and dissociative electron impact excitation to each of the investigated emission lines, an effective excitation rate $E^* = \sum_n f_n E_{i,n}$ is used which represents the sum over all electron impact excitation rates $E_{i,n}$ going into state i due to electron collisions with species n, where f_n is the fractional density of species n. Defining the dissociation degree (the density of atomic oxygen divided by that of molecular oxygen) as r_O allows the two considered effective excitation ratios to be written as

$$\frac{E^*_{750}}{E^*_{844}} = \frac{f_{Ar}}{f_{O2}} \frac{k_{750,d}(\varepsilon)}{r_O k_{844,d}(\varepsilon) + k_{844,de}(\varepsilon)}, \tag{6}$$

$$\frac{E^*_{777}}{E^*_{844}} = \frac{r_O k_{777,d}(\varepsilon) + k_{777,de}(\varepsilon)}{r_O k_{844,d}(\varepsilon) + k_{844,de}(\varepsilon)}. \tag{7}$$

Here, f_{O2} and f_{Ar} are the fractions of molecular oxygen and the argon tracer gas, and ε represents the local mean electron energy, corresponding to that of the EEDF calculated via the

Boltzmann solver. It should be noted that expressions (6) and (7) are only valid for small degrees of dissociation as they do not account for the depletion of the feed gas (in this case molecular oxygen) caused by dissociation. This assumption is well justified for the low power conditions considered in this work. The excitation ratios simulated via BOLSIG+ for a gas mixture of 98% O_2 and 2% Ar are shown as a function of dissociation degree and mean electron energy in Figs. 1(a) and 1(b). Figure 1(c) represents an overlay of the contour lines from Figs. 1(a) and 1(b). Each contour line represents a constant value of the respective excitation ratio. As such, the points at which the contour lines for each ratio cross define the dissociation degree and mean electron energy for those particular ratios. The dissociation degree and mean electron energy in the experiment are found by locating the crossing point of experimentally obtained excitation ratios in the same parameter space. It should be emphasised that the mean electron energy derived by this technique corresponds to an EEDF whose shape is determined by the solution of the two-term Boltzmann equation. As a result, the shape of the EEDF is variable and changes as the mean electron energy changes. As inputs for the two-term Boltzmann solver, the electron impact cross section set of Phelps has been used for molecular oxygen.[43,44] The electron impact reactions in this set include momentum transfer, dissociative electron attachment, electron impact ionization, and excitation into the oxygen metastable states $O_2(a^1\Delta_g)$ and $O_2(b^1\Sigma_g^+)$. Electronic excitation processes leading to electron energy losses of 4.5, 6.0, 8.4, and 9.97 eV are also included. These energy losses do not correspond to individual excited states, but rather represent cross sections with effective energy losses which have been derived so that the entire cross section set is consistent with measured electron transport data.[43] Additionally, the cross section for electron impact excitation of the $Ar(2p_1)$ state has been taken from Ref. 45 while those for direct and dissociative excitation of the $O(3p^3P)$ and $O(3p^5P)$ states are taken from Refs. 46 and 37. The importance of the choice of excitation cross sections for oxygen atom actinometry has been discussed in detail by Pagnon *et al.*[47] and it is clear that different combinations of cross sections can lead to the derivation of differing dissociation degrees and/or mean electron energies. The value of such an uncertainty is difficult to quantify; however, it is likely to be systematic and therefore the same for different experimental conditions and as a result still allows for accurate representation of experimental trends. Additionally, the choice of cross sections used in this work has been validated in a previous study where ERA was used to measure atomic oxygen densities in an atmospheric pressure plasma jet.[41] In that study, good agreement was found between atomic oxygen densities measured by ERA and those measured by TALIF.

The influence of the 2% Ar admixture on the optical emission of the plasma was investigated by comparing the emission from the $O(3p^3P)$ and $O(3p^5P)$ states for plasmas composed of pure O_2 and 98% O_2 and 2% Ar. Any differences in both the time and space averaged and time and space resolved emission were found to be negligible. This implies that the mean electron energy and the EEDF are not strongly influenced by the presence of the 2% Ar admixture which is consistent with electron energy losses being dominated by inelastic collisions with oxygen molecules. The influence of the small argon admixture on the dissociation degree is also expected to be minor based on the work of Kitajima *et al.*[48]

In this work, ERA is applied to investigate the radial distribution of the oxygen dissociation degree and local mean electron energy in low pressure capacitively coupled radio frequency (rf) oxygen plasmas in contact with surfaces consisting of two common components of wafers used in the microelectronics industry, namely, copper and silicon dioxide. The experimental set-up is described in Section II. Section III describes the extraction of the excitation ratios from the Phase Resolved Optical Emission Spectroscopy (PROES) measurements and Section IV discusses the observed radial profiles of the oxygen dissociation degree and the local mean electron energy for the two surface materials at different pressures and driving voltages. The implications of the observed trends for plasma processing applications are also discussed.

II. EXPERIMENTAL SETUP

The plasma is produced in a Gaseous Electronics Conference (GEC) reference cell.[49] The details of the electrode geometry are shown in detail in Fig. 2(a). The geometry resembles the inductively coupled version of the GEC cell; however, in this work it is operated in capacitive mode by powering the bottom (usually grounded) electrode which

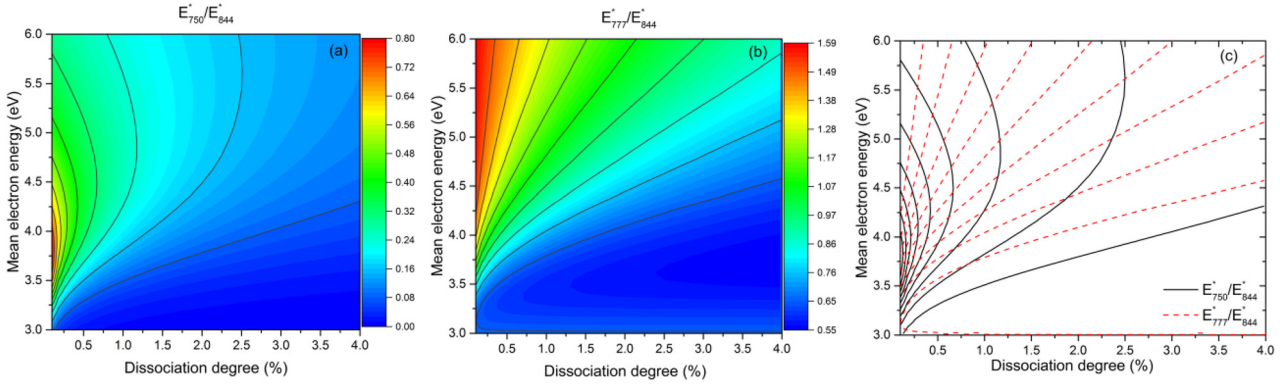

FIG. 1. Calculated effective excitation ratios ((a) and (b)) as a function of dissociation degree and mean electron energy. (c) represents an overlay of the contour lines for both excitation ratios shown in (a) and (b). These excitation ratios are obtained for 98% O_2 and 2% Ar.

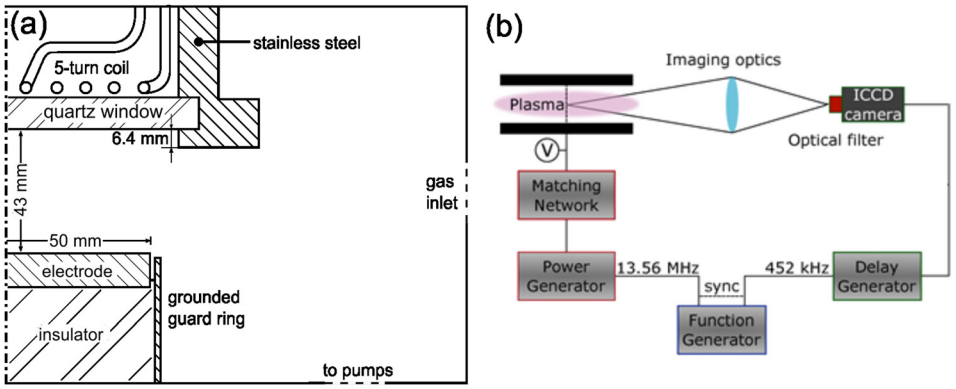

FIG. 2. (a) Close-up schematic of the electrode geometry of the GEC reference cell used in this work. (b) Schematic of the ICCD camera set-up.

has a diameter of 102 mm with a driving frequency of 13.56 MHz. The top coil is grounded. The gap between the dielectric window that separates the top coil from the plasma volume and the powered electrode is 43 mm. Using this gap distance at the relatively high pressures considered in this work, the plasma exhibits a strong asymmetry with the peak plasma emission occurring close to the powered electrode. As a result, the role played by the dielectric window in defining the plasma characteristics is expected to be minor. Flow rates of O_2 and tracer gas Ar were maintained at 50 sccm (standard cubic centimetres per minute) and 1 sccm, respectively. The applied voltage at the lower electrode was measured using a capacitive voltage probe (LeCroy PPE 20 kV). Typical voltage amplitudes applied to the lower electrode in this work range from 200 to 400 V. The corresponding power measured by the rf generator ranges from around 20 to 80 W. In order to change the surface material, discs consisting of different materials of 100 mm diameter were placed on the lower electrode. These discs are placed such that a 1 mm gap remains around the circumference of the powered electrode. The materials investigated were silicon dioxide (SiO_2 50 nm on a 0.5 mm thick (100) Si wafer) and copper (Cu, 1 mm thick, unpolished). It should be noted that after the measurements using each material were completed the surfaces of the materials were found to be visibly altered by the plasma treatment. This was particularly noticeable around the edges of each disc which were visibly darker in each case. This is likely related to enhanced ion bombardment at the electrode edges due to edge effects occurring in the design of the GEC reference cell.[50] More specifically, the SiO_2 was highly reflective before plasma exposure and became less reflective afterwards. The copper surface was unpolished before plasma exposure, and thus not very reflective. However, after exposure to the plasma the copper surface became highly reflective.

As shown schematically in Fig. 2(b), a function generator (TTi 100 MHz Arbitrary Waveform Generator TGA-12104) is used to provide synchronized trigger signals for the power and delay generators, respectively. A sinusoidal trigger signal at 13.56 MHz is used to synchronise the function generator with a fixed frequency power generator (Coaxial Power Systems RFG 150-13) and a rectangular trigger signal at 452 kHz is used to synchronise with the delay generator (Stanford Research Systems DG 645). A matching network (Coaxial Power Systems MMN 150-13) is used to match the impedance of the discharge to the output impedance of the power generator, so that rf power is coupled efficiently into the discharge such that the reflected power stays below 1%.

The delay generator creates a trigger signal, which is synchronised to the rf driving voltage waveform, for the intensified charge-coupled device (ICCD) camera (Andor iStar DH344T-18U-73) with a variable delay which is used to scan through the rf period at intervals of 2 ns. The trigger frequency for the ICCD camera is limited to 500 kHz by specification; therefore, a frequency of 452 kHz is chosen which is exactly 1/30 of the driving frequency, this is necessary to avoid the trigger signal and the rf waveform from drifting in time with respect to one another. For time-resolved monitoring of the signals, a digital storage oscilloscope (LeCroy WaveSurfer 104 MXs-B 1 GHz) is used.

Two-dimensional measurements were carried out using custom optical narrow bandpass filters (LOT-QuantumDesign: 750.46 ± 0.50 nm; 777.45 ± 1.75 nm; 844.79 ± 0.95 nm) to obtain wavelength selectivity. The very narrow bandwidth of each filter allows for high spectral selectivity compared to more commonly used optical filters which typically have spectral transmission functions with full-width-half-maxima of 5–10 nm. By using an optical filter with a such a narrow spectral transmission function it is possible, for example, to differentiate between emission at 750.46 nm, corresponding to the $Ar(2p_1)$ state, and emission at 751.5 nm, corresponding to the $Ar(2p_5)$ state which is not possible using optical filters with broader spectral transmission functions. This is important because the electron impact excitation cross sections for the two upper states are different[45] so proper selectivity between them is necessary to obtain maximum accuracy when comparing measured excitation ratios with simulated excitation ratios which depend on the electron impact excitation cross section. The spatial resolution of the optical set-up is around 100 μm. To obtain the radial distribution of the dissociation degree and local mean electron energy above the powered electrode, the two-dimensional optical emission measurements were divided into 19 columns radially (1 central column and 9 columns on each side of the centre). This gives a final spatial resolution of $\approx$5 mm. Since the discharge is symmetric in the radial direction, the results from both sides were averaged. The number of bins is chosen to balance the need for a good signal-to-noise ratio, which increases with the size of each bin, with the requirement to properly resolve the radial profiles of the derived quantities.

III. DETERMINATION OF EXCITATION RATIOS, DISSOCIATION DEGREE, AND LOCAL MEAN ELECTRON ENERGY

The excitation dynamics of each state of interest were determined from the measured phase resolved optical emission and the excitation function[51–54] which is given as

$$E_i(t,x) = \frac{1}{n_0}\left(\frac{dn_i(t,x)}{dt} + \frac{1}{\tau_{eff}} n_i(t,x)\right), \tag{8}$$

$$\text{where} \quad n_i(t,x) = \frac{I_i(t,x)}{A_{ik}}. \tag{9}$$

Here, n_i represents the excited state density, and τ_{eff} is the effective lifetime of the excited state, taking into account collisional quenching and is given by

$$\tau_{eff} = \frac{1}{A_i + Q_i}. \tag{10}$$

Molecular oxygen is assumed to be the dominant quenching partner for each of the three excited states considered. As such Q_i is calculated using the quenching coefficients k_{iq} (see Eq. (3)) for the three excited states in collisions with molecular oxygen. The values used are 7.6×10^{-16} m^3 s^{-1}, 9.4×10^{-16} m^3 s^{-1}, and 10.6×10^{-16} m^3 s^{-1} and are taken from Refs. 55–57 for the Ar($2p_1$), O($3p^3$P), and O($3p^5$P), respectively. The gas temperature above the powered electrode was determined spectroscopically from rotational band emission of nitrogen, added as an impurity, and depending on the operating conditions was found to vary between around 350 and 450 K. For a given pressure and power, the gas temperature was found to be the same, within the uncertainty of the measurement, for the different surface materials investigated. As such the molecular oxygen density required for the calculation of Q_i is determined from the ideal gas law at a temperature of 400 K for each considered pressure. For a given condition, the gas temperature was found to remain independent of radial position, within the uncertainty associated with the measurement. Figure 3 shows typical examples of the temporally and spatially resolved (a) emission at $\lambda = 750.46$ nm and (b) excitation of the Ar($2p_1$) state throughout one rf cycle at 13.56 MHz over an SiO_2 surface. Both are normalised to their maximum values. Here, the maxima in emission and excitation intensity occur as a result of the expanding sheath motion at a time of 15–20 ns and a distance of around 8 mm from the powered electrode. This pattern of spatially and temporally resolved excitation is typical of an oxygen discharge operated in the low power α mode.[58,59] Throughout this investigation the highest excitation rate, for all three excited states studied and for all combinations of voltage, pressure and surface material, was found to occur as a result of sheath expansion electron heating. The spatio-temporal coordinates, from which the excitation ratios used in the derivation of the dissociation degree and local mean electron energy are extracted, are chosen to maximise the signal-to-noise ratio and minimise the contribution of indirect processes, such as cascades from higher excited levels. The optimal coordinates from this perspective were found to occur at the spatial coordinate of the maximum excitation and the temporal coordinate just before the maximum excitation. Spatially this corresponds to an axial coordinate around 8 mm from the powered electrode for the conditions shown in Fig. 3. In this region of space and time, electrons are strongly heated by the expanding sheath edge at the powered electrode. As such, the mean electron energy is high meaning that the electron impact excitation rate of the considered excited states is high and the contribution of cascades to the population of these excited states is low. At other points in space and time where electrons are not being heated strongly and the mean electron energy is lower, the contribution of electron impact excitation is smaller and cascade processes from higher levels, excited by electron impact at earlier times, have a more significant contribution to the observed emission. This is due to the delay in the emission originating from higher levels caused by the requirement that the upper cascading states must first transition to the lower state which emits at the observed wavelengths.

IV. RADIAL DISTRIBUTION OF DISSOCIATION DEGREE AND LOCAL MEAN ELECTRON ENERGY

In this section, we focus on two materials which are commonly used as wafer components in the microelectronics industry, Cu and SiO_2. Figure 4 shows the measured radial distribution of the oxygen dissociation degree and the local mean electron energy at sheath expansion at a pressure of 40 Pa and an applied voltage of 200 V for both Cu and SiO_2. The error bars shown are as a result of experimental

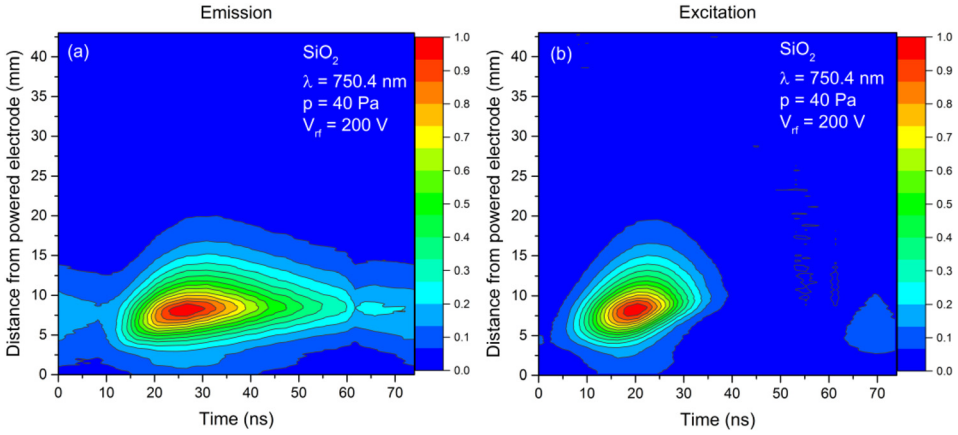

FIG. 3. Typical example of temporally and spatially resolved (a) emission at $\lambda = 750.46$ nm and (b) excitation of the Ar($2p_1$) state over an SiO_2 surface ($V_{rf} = 200$ V, 98% O_2, and 2% Ar).

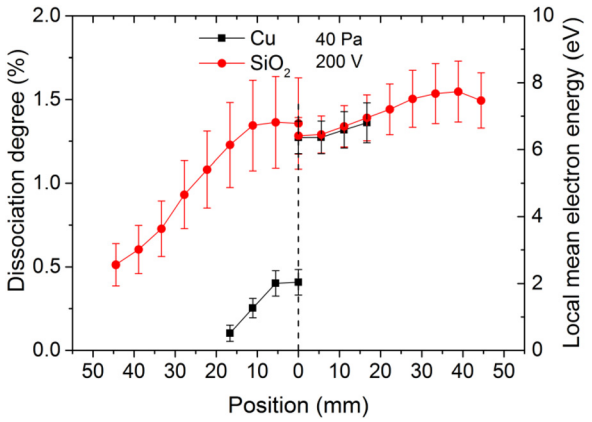

FIG. 4. Radial distribution of the oxygen dissociation degree and the local mean electron energy for Cu and SiO_2 surfaces ($V_{rf} = 200$ V, $p = 40$ Pa, 98% O_2, and 2% Ar).

uncertainties and have been determined based on the uncertainty in the measured excitation ratios corresponding to typical signal-to-noise ratios obtained from the ICCD images. The final error bars correspond to the uncertainty in the dissociation degree and local mean electron energy associated with the determination of the crossing point of each excitation ratio induced by the uncertainty in the signal-to-noise ratio. The same methodology has been used to determine the uncertainty in the dissociation degree and local mean electron energy shown in Figs. 5 and 6. Additional systematic uncertainties will be present due to uncertainties in the electron impact cross sections used to simulate the values of the excitation ratios. The uncertainties in the measured electron impact cross sections are around 20% and 15% for direct excitation of the $Ar(2p_1)$ level[45] and dissociative excitation of the $O(3p^3P)$ and $O(3p^5P)$ levels,[37] respectively. For direct excitation of the $O(3p^3P)$ and $O(3p^5P)$, Ref. 46 does not specify uncertainties; however, these are also expected to be on the order of 20%. Thus, an estimate of the minimum systematic uncertainty in the dissociation degree and mean electron energy induced by uncertainties in the electron impact cross sections can be given as 20–30%. This additional uncertainty will remain the same for the different experimental conditions and as a result does not affect the observed trends and comparisons of the surface materials with respect to one another.

The dissociation degrees shown in Figs. 4 and 5 are on the order of 0.1–1.5%. These are consistent with the values found by previous studies which have used TALIF to measure atomic oxygen densities under similar conditions in similar reactors.[32,34,60] This consistency with TALIF measurements is in accordance with the results of our previous work which showed good agreement between atomic oxygen densities measured by ERA and TALIF in an atmospheric pressure plasma jet.[41]

In Fig. 4, it is observed that the dissociation degree is a factor of 2–3 higher for SiO_2 than for Cu at the radial centre of the electrode. In both cases, the dissociation degree exhibits a dome shaped profile with a maximum in the centre decreasing with distance from the electrode centre. In the case of Cu, it was not possible to reliably determine crossing points for the two excitation ratios at radial distances greater than or equal to 20 mm from the electrode centre. This reflects the fact that the dissociation degree has decreased below the minimum which can reliably be detected with this technique. This minimum value is around 0.1%. As a result, no dissociation degree or local mean electron energy has been plotted for Cu at distances greater than or equal to 20 mm. In the case of SiO_2, the radial profile is in accordance with previous works which have measured the radially resolved fluorescence of atomic oxygen using TALIF in a similar system, albeit with a different surface material.[61,62] The decreased dissociation degree at the electrode edge is most likely related to a decreasing electron density in this region due to radial diffusion of electrons towards the chamber walls and therefore lower electron impact dissociation rates.

Under the conditions considered in this work, the loss of atomic oxygen is dominated by recombination at the reactor walls. This is demonstrated by considering the importance of various loss processes for atomic oxygen. Using the expression derived by Chantry[63] and Booth and Sadeghi[22] for the wall loss rate of a given species k_{wall}

$$\frac{1}{k_{wall}} = \frac{\Lambda_0^2}{D} + \frac{V}{A}\frac{2(2-\gamma)}{\bar{v}\gamma}, \tag{11}$$

where γ is the wall recombination coefficient of atomic oxygen, V and A are the volume and surface area of the reactor, respectively, and $\bar{v}$ and D are the mean velocity and diffusion coefficients of atomic oxygen. Λ_0^2 is the diffusion length defined for a cylinder as

$$\frac{1}{\Lambda_0^2} = \left(\frac{\pi}{L}\right)^2 + \left(\frac{2.405}{r}\right)^2, \tag{12}$$

where L is the length of the cylinder and r is the radius. Using the expression for the diffusion coefficient of a species in a binary mixture given in Ref. 64 the diffusion coefficient of atomic oxygen in molecular oxygen is expressed as

$$D = \frac{3}{8 n_{O2}\sigma_{12}^2}\sqrt{\frac{k_B T}{2\pi}\left(\frac{1}{m_O} + \frac{1}{m_{O2}}\right)}, \tag{13}$$

where n_{O2} is the density of molecular oxygen, $\sigma_{12} = (\sigma_1 + \sigma_2)/2$, where σ_1 and σ_2 are the Lennard Jones collision cross sections for atomic and molecular oxygen. m_O and m_{O2} are the masses of atomic and molecular oxygen, respectively. The mean velocity of oxygen atoms, $\bar{v} = \sqrt{(8k_B T)/\left(\frac{\pi}{m_O}\right)}$. Using $\gamma = 0.01$, which is on the lower end of the range of values measured in the literature for conditions similar to those in this work, for a pressure of 40 Pa and gas temperature of 400 K, equation 11 yields a value of $k_{wall} \approx 140\ s^{-1}$. This loss rate is significantly higher than those through other processes under our conditions. For example, the gas residence time in our reactor is ≈0.3 s giving a loss rate through pumping of $\approx 3\ s^{-1}$. The destruction of atomic oxygen through ozone formation via a three-body process with two oxygen molecules has a much lower rate of $\approx 0.01\ s^{-1}$ based on the rate coefficient given in Ref. 65.

Electron impact excitation of ground state atomic oxygen into the ^1D or ^1S states is also a negligible loss process of ground state atomic oxygen at the low electron densities expected in the low power capacitively coupled plasmas considered in this work.

Given that surface losses of atomic oxygen are dominant under the conditions studied in this work, the overall lower dissociation degree for Cu as compared to SiO_2 is in accordance with previous measurements of the atomic oxygen surface recombination coefficient carried out by Guha *et al.*[17] In that study, the authors found that the recombination coefficient for atomic oxygen on SiO_2 surfaces increased from ≈0.04 to ≈0.07 when Cu was deposited on the surface. The lower dissociation degree for Cu as compared to SiO_2 surfaces observed in this work offers further confirmation of the importance of Cu chamber wall coatings in defining atomic oxygen densities in plasma reactors. Over the radial distance range for which results have been determined for both materials, the local mean electron energies are identical, within the experimental uncertainties. This similarity in mean electron energies offers further confirmation that the difference in the dissociation degree between the two materials is related to differing surface recombination of atomic oxygen and not changes in other plasma parameters. For both surface materials, the local mean electron energy is observed to increase slightly with distance from the centre of the electrode, taking a maximum at the electrode edge. This is more clearly observed for SiO_2 where the full radial profile can be determined. This maximum is a consequence of edge effects which are known to occur in the GEC reference cell design.[50] These edge effects result in strong electric fields at the electrode edge formed between the grounded guard ring and the powered electrode[50] which can lead to higher electron temperatures.

Figure 5 shows the radial distribution of local mean electron energy and dissociation degree at an increased pressure of 80 Pa and the same applied voltage amplitude of 200 V. It is observed that, on average, the local mean electron energies are lower for both surface materials at a pressure of 80 Pa than for the same voltage at a pressure of 40 Pa, with the SiO_2 surface leading to slightly higher local mean electron energies. The decreases in local mean electron energy for both materials with increasing pressure are a result of the higher electron collision frequencies at higher pressure which leads to electrons losing more energy through collisions with the background gas. A decrease in mean electron energy as the pressure is increased at constant voltage is in accordance with the results of one-dimensional Particle-in-Cell (PIC) simulations of an oxygen capacitively coupled plasma (CCP) carried out recently by Gudmundsson and Ventéjou.[66] In the case of SiO_2, the oxygen dissociation degree is similar at both 40 Pa and 80 Pa, whereas in the case where the Cu surface is used the dissociation degree has increased compared to the 40 Pa case. A possible explanation for the increase in dissociation degree in the case of the Cu surface as compared to SiO_2 surface may be the decreased importance of atomic oxygen surface recombination at higher pressures, the result being that the dissociation degree for both materials approaches the same value as the pressure is increased. There may be multiple reasons for such a pressure dependence. At higher pressures, the rate of diffusion of atomic oxygen to the surface will decrease and as a result, surface losses of atomic oxygen will decrease with increasing pressure for both materials. Additionally, surface recombination probabilities for atomic oxygen in plasma reactors are known to decrease with increasing pressure.[12] The combination of both factors would tend to decrease the importance of surface processes as loss channels for atomic oxygen with increasing pressure, the result being that the surface in contact with the plasma has less influence on the dissociation degree.

Figure 6 shows the radial distribution of local mean electron energy and dissociation degree at a pressure of 40 Pa and voltage amplitude of 400 V. By comparison with Fig. 4, the role of the increasing voltage amplitude in the dissociation degree and mean electron energy can be observed. It is found that both the dissociation degree and the local mean electron energy increase as the driving voltage amplitude is increased from 200 V to 400 V. Under these conditions, both parameters are found to be the same for Cu and SiO_2, within the uncertainty associated with the measurements. The increase in the local mean electron energy under

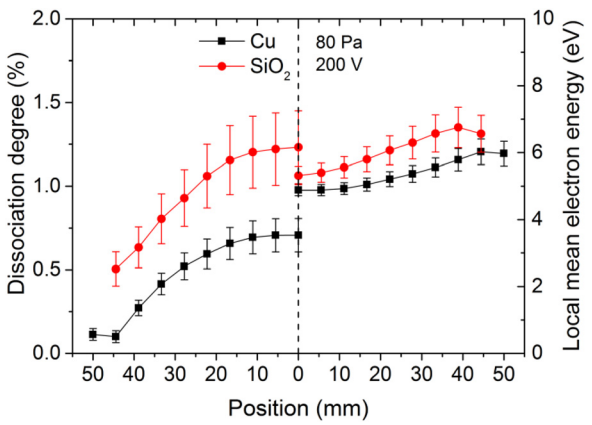

FIG. 5. Radial distribution of the oxygen dissociation degree and the local mean electron energy for Cu and SiO_2 surfaces ($V_{rf} = 200$ V, $p = 80$ Pa, 98% O_2, and 2% Ar).

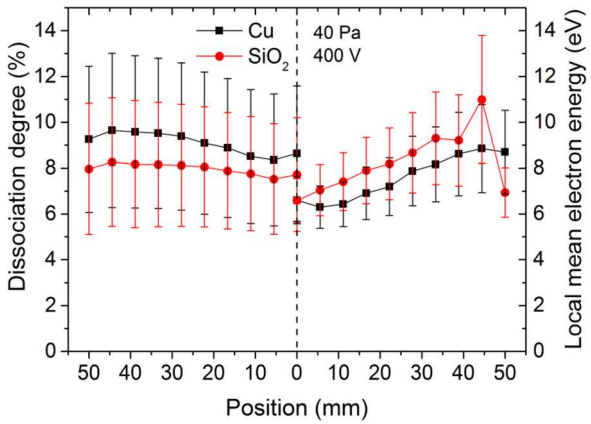

FIG. 6. Radial distribution of the oxygen dissociation degree and the local mean electron energy for Cu and SiO_2 surfaces ($V_{rf} = 400$ V, $p = 40$ Pa, 98% O_2, and 2% Ar).

these high voltage conditions reflects the increased importance of secondary electrons emitted from the electrode surfaces and accelerated inside the plasma sheath. These electrons have higher energy than those formed in the plasma bulk due to their acceleration through the plasma sheath and as a result, the local mean electron energy derived is higher than for the lower voltage case where fewer of these electrons are present. The increase in dissociation degree is a reflection of the higher power deposition as the voltage is increased. The power deposited in the plasma, and therefore the electron density, typically scale with the square of the voltage.[67,68] The dominant formation pathway of atomic oxygen is through direct electron-impact dissociation of the oxygen background gas and as a result, the dissociation degree also follows the electron density and thus scales as the square of the voltage. The increased mean electron energy at higher voltages will have the effect of further increasing the dissociation degree as higher mean electron energies mean that a higher proportion of electrons have the energy required to dissociate the oxygen molecule leading to a higher electron impact dissociation rate coefficient. It is notable that the higher voltage case appears to result in a flatter profile of the dissociation degree as a function of radial position.

V. CONCLUSIONS

The presented Energy Resolved Actinometry (ERA) has been used to measure the oxygen dissociation degree as well as the local mean electron energy simultaneously in technologically relevant oxygen CCPs in contact with copper and silicon dioxide surfaces. The presented technique allows for sensitive measurement of the two quantities with high spatial resolution ($\approx$5 mm). The measurement of both quantities simultaneously allows for increased insight into the fundamental processes occurring in oxygen CCPs compared to alternative techniques where only one or the other quantity is measured.

It has been observed that the dissociation degree takes on a dome shaped radial profile, with a peak at the radial centre of the electrode surface at low driving voltages for both materials investigated. Conversely, the local mean electron energy follows an increasing trend with distance from the radial centre of the electrodes, taking its maximum value near the electrode edge. This has been attributed to electrode edge effects, known to occur in the GEC reference cell design. In addition, it has been found that the dissociation degree is significantly higher in the case where the plasma is in contact with a SiO_2 surface as compared to a Cu surface. This is in accordance with previous determinations of the surface recombination probability of atomic oxygen on both surfaces.[17] The difference in the dissociation degree between the two surfaces was found to decrease with increasing pressure, suggesting that surface recombination of atomic oxygen becomes a less important loss channel at higher pressure. Furthermore, the local mean electron energies were determined to be the same within the experimental uncertainties for both surface materials under both low and high voltage conditions at 40 Pa, with a small difference observed at 80 Pa. Under higher voltage conditions, both the dissociation degree and local mean electron energy were found to increase, in accordance with higher power deposition and an increased contribution of secondary electrons to the electron dynamics of the plasma. Interestingly, the radial profile of the dissociation degree has been found to be flatter under higher voltage conditions, which may be of interest from the perspective of improving the radial uniformity of surface modifications in the plasma processing industry. Additionally, from a plasma processing perspective this work confirms the importance of atomic oxygen surface recombination probabilities in determining the characteristics of the plasma, particularly with regard to the dissociation fraction. The presented technique is expected to be a valuable tool to further understanding of the complex spatial profiles of electron heating and reactive species densities in industrial plasma reactors. Such knowledge is of key importance for the development of next generation of industrial plasma processes.

ACKNOWLEDGMENTS

The authors acknowledge Intel Ireland, Ltd. for financial support and the U.K. Engineering and Physical Sciences Research Council (EPSRC) for supporting this research through the EPSRC Manufacturing Grant (No. EP/K018388/1) and the EPSRC Career Acceleration Fellowship (EP/H003797/1). The authors would also like to thank Dr. Andrew West and Dr. Christopher Bowman for useful discussions during the preparation and writing of this article.

[1]M. A. Hartney, D. W. Hess, and D. S. Soane, J. Vac. Sci. Technol., B **7**, 1 (1989).
[2]C. J. Mogab, A. C. Adams, and D. L. Flamm, J. Appl. Phys. **49**, 3796 (1978).
[3]R. d'Agostino, F. Cramarossa, S. De Benedictis, and G. Ferraro, J. Appl. Phys. **52**, 1259 (1981).
[4]D. A. Carl, D. W. Hess, and M. A. Lieberman, J. Appl. Phys. **68**, 1859 (1990).
[5]A. West, M. van der Schans, C. Xu, M. Cooke, and E. Wagenaars, Plasma Sources Sci. Technol. **25**, 02LT01 (2016).
[6]B. G. Heil, U. Czarnetzki, R. P. Brinkmann, and T. Mussenbrock, J. Phys. D: Appl. Phys. **41**, 165202 (2008).
[7]B. Bruneau, T. Gans, D. O'Connell, A. Greb, E. V. Johnson, and J. P. Booth, Phys. Rev. Lett. **114**, 125002 (2015).
[8]A. R. Gibson, A. Greb, W. G. Graham, and T. Gans, Appl. Phys. Lett. **106**, 054102 (2015).
[9]E. Schüngel, S. Mohr, J. Schulze, and U. Czarnetzki, Appl. Phys. Lett. **106**, 054108 (2015).
[10]T. Lafleur, Plasma Sources Sci. Technol. **25**, 013001 (2016).
[11]S. Rajendiran, A. Rossall, A. R. Gibson, and E. Wagenaars, Surf. Coat. Technol. **260**, 417–423 (2014).
[12]S. Gomez, P. G. Steen, and W. G. Graham, Appl. Phys. Lett. **81**, 19 (2002).
[13]A. Greb, K. Niemi, D. O'Connell, and T. Gans, Appl. Phys. Lett. **103**, 244101 (2013).
[14]A. Greb, A. R. Gibson, K. Niemi, D. O'Connell, and T. Gans, Plasma Sources Sci. Technol. **24**, 044003 (2015).
[15]J. C. Greaves and J. W. Linnett, Trans. Faraday Soc. **55**, 1355 (1959).
[16]L. Stafford, J. Guha, R. Khare, S. Mattei, O. Boudreault, B. Clain, and V. M. Donnelly, Pure Appl. Chem. **82**, 1301 (2010).
[17]J. Guha, R. Khare, L. Stafford, V. M. Donnelly, S. Sirard, and E. A. Hudson, J. Appl. Phys. **105**, 113309 (2009).
[18]A. Agarwal and M. J. Kushner, J. Vac. Sci. Technol., A **26**, 498 (2008).
[19]G. Cunge, O. Joubert, and N. Sadeghi, J. Appl. Phys. **94**, 6285 (2003).
[20]G. P. Kota, J. W. Coburn, and D. B. Graves, J. Vac. Sci. Technol., A **16**, 270 (1998).

[21]J. P. Booth, O. Joubert, J. Pelletier, and N. Sadeghi, J. Appl. Phys. **69**, 618 (1991).
[22]J. P. Booth and N. Sadeghi, J. Appl. Phys. **70**, 611 (1991).
[23]T. Kitajima, K. Noro, T. Nakano, and T. Makabe, J. Phys. D: Appl. Phys. **37**, 2670 (2004).
[24]H. Singh, J. W. Coburn, and D. B. Graves, J. Appl. Phys. **88**, 3748–3755 (2000).
[25]A. R. Gibson, M. Foucher, D. Marinov, P. Chabert, T. Gans, M. J. Kushner, and J.-P. Booth, Plasma Phys. Controlled Fusion **59**, 024004 (2017).
[26]G. S. Selwyn, J. Appl. Phys. **60**, 2771 (1986).
[27]R. E. Walkup, K. L. Saenger, and G. S. Selwyn, J. Chem. Phys. **84**, 2668 (1986).
[28]E. J. H. Collart, J. A. G. Baggerman, and R. J. Visser, J. Appl. Phys. **70**, 5278 (1991).
[29]A. Goehlich, T. Kawetzki, and H. F. Döbele, J. Chem. Phys. **108**, 9362–9370 (1998).
[30]N. Knake, S. Reuter, K. Niemi, V. Schulz-von der Gathen, and J. Winter, J. Phys. D: Appl. Phys. **41**, 194006 (2008).
[31]J. W. Coburn and M. Chen, J. Appl. Phys. **51**, 3134 (1980).
[32]H. M. Katsch, A. Tewes, A. Goehlich, T. Kawetzki, E. Quandt, and H. F. Döbele, J. Appl. Phys. **88**, 6232 (2000).
[33]K. Niemi, S. Reuter, L. M. Graham, J. Waskoenig, and T. Gans, Appl. Phys. Lett. **95**, 151504 (2009).
[34]J. Conway, S. Kechkar, N. O'Connor, C. Gaman, M. M. Turner, and S. Daniels, Plasma Sources Sci. Technol. **22**, 045004 (2013).
[35]H. Nagai, M. Hiramatsu, M. Hori, and T. Goto, Rev. Sci. Instrum. **74**, 3453 (2003).
[36]K. Niemi, D. O'Connell, N. de Oliveira, D. Joyeux, L. Nahon, J. P. Booth, and T. Gans, Appl. Phys. Lett. **103**, 034102 (2013).
[37]M. B. Schulman, F. A. Sharpton, S. Chung, C. C. Lin, and L. W. Anderson, Phys. Rev. A **32**, 2100 (1985).
[38]M. Abdel-Rahman, V. Schulz-von der Gathen, T. Gans, K. Niemi, and H. F. Döbele, Plasma Sources Sci. Technol. **15**, 620 (2006).
[39]M. Foucher, D. Marinov, E. Carbone, P. Chabert, and J.-P. Booth, Plasma Sources Sci. Technol. **24**, 042001 (2015).
[40]T. Wegner, C. Küllig, and J. Meichsner, Plasma Sources Sci. Technol. **26**, 025006 (2017).
[41]A. Greb, K. Niemi, D. O'Connell, and T. Gans, Appl. Phys. Lett. **105**, 234105 (2014).
[42]G. J. M. Hagelaar and L. C. Pitchford, Plasma Sources Sci. Technol. **14**, 722 (2005).
[43]S. Lawton and A. Phelps, J. Chem. Phys. **69**, 1055–1068 (1978).
[44]See www.lxcat.net for Phelps database; accessed 27 September 2010.
[45]J. E. Chilton, J. B. Boffard, R. S. Schappe, and C. C. Lin, Phys. Rev. A **57**, 267 (1998).
[46]R. R. Laher and F. R. Gilmore, J. Phys. Chem. Ref. Data **19**, 277–305 (1990).
[47]D. Pagnon, J. Amorim, J. Nahorny, M. Touzeau, and M. Vialle, J. Phys. D: Appl. Phys. **28**, 1856–1868 (1995).
[48]T. Kitajima, T. Nakano, and T. Makabe, Appl. Phys. Lett. **88**, 091501 (2006).
[49]P. A. Miller, G. A. Hebner, K. E. Greenberg, P. D. Pochan, and B. P. Aragon, J. Res. Natl. Inst. Stand. Technol. **100**, 427 (1995).
[50]U. Czarnetzki, D. Luggenhölscher, and H. F. Döbele, Plasma Sources Sci. Technol. **8**, 230 (1999).
[51]C. M. O. Mahony, R. Al Wazzan, and W. G. Graham, Appl. Phys. Lett. **71**, 608 (1997).
[52]T. Gans, V. Schulz-von der Gathen, and H. F. Döbele, Contrib. Plasma Phys. **44**, 523 (2004).
[53]J. Schulze, E. Schüngel, Z. Donkó, D. Luggenhölscher, and U. Czarnetzki, J. Phys. D: Appl. Phys. **43**, 124016 (2010).
[54]T. Gans, D. O'Connell, V. Schulz-von der Gathen, and J. Waskoenig, Plasma Sources Sci. Technol. **19**, 034010 (2010).
[55]N. Sadeghi, D. W. Setser, A. Francis, U. Czarnetzki, and H. F. Döbele, J. Chem. Phys. **115**, 3144 (2001).
[56]K. Niemi, V. Schulz-von der Gathen, and H. F. Döbele, Plasma Sources Sci. Technol. **14**, 375 (2005).
[57]P. J. Dagdigian, B. E. Forch, and A. W. Miziolek, Chem. Phys. Lett. **148**, 299 (1988).
[58]K. Dittmann, D. Drozdov, B. Krames, and J. Meichsner, J. Phys. D: Appl. Phys. **40**, 6593 (2007).
[59]C. Dittmann, C. Küllig, and J. Meichsner, Plasma Phys. Controlled Fusion **54**, 124038 (2012).
[60]C. S. Corr, S. Gomez, and W. G. Graham, Plasma Sources Sci. Technol. **21**, 055024 (2012).
[61]M. Geigl, S. Peters, O. Gabriel, B. Krames, and J. Meichsner, Contrib. Plasma Phys. **45**, 369–377 (2005).
[62]C. Küllig, T. Wegner, and J. Meichsner, Plasma Sources Sci. Technol. **24**, 015027 (2015).
[63]P. J. Chantry, J. Appl. Phys. **62**, 1141–1148 (1987).
[64]S. Chapman and T. G. Cowling, *The Mathematical Theory of Non-Uniform Gases*, 3rd ed. (Cambridge University Press, 1970).
[65]J. B. Burkholder, S. P. Sander, J. P. D. Abbat, J. R. Barker, R. E. Huie, C. Kolb, M. J. Kurylo, V. L. Orkin, D. M. Wilmouth, and P. H. Wine, *Chemical Kinetics and Photochemical Data for Use in Atmospheric Studies* (Jet Propulsion Laboratory, Pasadena, 2015).
[66]J. T. Gudmundsson and B. Ventéjou, Plasma Sources Sci. Technol. **118**, 153302 (2015).
[67]V. A. Godyak, R. B. Piejak, and B. M. Alexandrovich, IEEE Trans. Plasma Sci. **19**, 660–676 (1991).
[68]T. Lafleur, P. A. Delattre, J. P. Booth, E. V. Johnson, and S. Dine, Rev. Sci. Instrum. **84**, 015001 (2013).